

Preparation and magnetoresistance behavior of nickel nanoparticles embedded in hydrogenated carbon film

Mehrdad Molamohammadi¹ · Carlos Luna² · Ali Arman¹ · Shahram Solaymani¹ · Arash Boochani³ · Azin Ahmadpourian³ · Azizollah Shafiekhani^{4,5}

Received: 30 April 2015 / Accepted: 30 May 2015 / Published online: 12 June 2015
© Springer Science+Business Media New York 2015

Abstract Nickel nanoparticles arrays, growth into hydrogenated amorphous carbon, were prepared by means of RF-plasma enhanced chemical vapor deposition and RF-sputtering co-deposition from acetylene and a nickel target. The resulting nanocomposite films were characterized by X-ray diffraction and atomic force microscopy, and their magnetic responses and magnetoresistance behavior were investigated as a function of the exciting magnetic field and the Ni nanoparticles content, which was conveniently controlled by adjusting the deposition time. These physical properties were explained by a combination of hopping and tunneling effects.

1 Introduction

Nanostructure materials are crucial elements for the advance of several scientific disciplines and the development of innovative devices [1]. The interest of these

systems is largely due to their size-dependent physico-chemical properties that can be rather different than those observed in their bulk analogous, and which can be uniquely tailored for various types of applications by properly selecting their composition, structure, size and morphology and the particle arrangement. In this regards, arrays of fine magnetic nanoparticles are of huge current importance due to the understanding of their magnetic phenomenology is essential for the progress of the physics of magnetism and the advance of revolutionary technologies such as ultrahigh-density magnetic recording media [2], nanomedicine [3–5] and spintronics [6].

Nowadays, given the development of more and more advanced preparation techniques, there is a large variety of methods based on top-down and bottom-up approaches that allow the preparation of two-dimensional arrays of magnetic nanoparticles with different morphologies, compositions and structures [2, 7–11]. In this matter, the sputtering [12, 13] and the chemical vapor deposition techniques [14] have been especially relevant, and their versatility have recently combined to prepare nanocomposite films [15–20].

In this article we study the magnetic response and the magnetoresistance behavior at room temperature of nanocomposite films constituted by fine nickel nanoparticles embedded into hydrogenated amorphous carbon prepared by a combination of plasma enhanced chemical vapor deposition (RF-PECVD) and RF-sputtering. The morphology and the crystal structure were analyzed by atomic force microscopy (AFM) and X-ray diffraction (XRD), respectively, and the effects of the Ni concentration nanoparticles and the applied magnetic field on magnetization and transport measurements have been investigated.

✉ Ali Arman
ali.arman173@gmail.com; Ali.gelali@gmail.com

¹ Young Researchers and Elite Club, Kermanshah Branch, Islamic Azad University, Kermanshah, Iran

² Facultad de Ciencias Físico Matemáticas, Universidad Autónoma de Nuevo León, Av. Pedro de Alba s/n, 66455 San Nicolás de los Garza, Nuevo León, Mexico

³ Department of Physics, Kermanshah Branch, Islamic Azad University, Kermanshah, Iran

⁴ School of Physics, Institute for Research in Fundamental Sciences, P.O. Box 19395-5531, Tehran, Iran

⁵ Physics Department, Alzahra University, 1993893973 Tehran, Iran

2 Experimental details

Arrays of nickel nanoparticles (Ni NPs) on carbon substrates with different Ni NPs concentrations were grown using simultaneously RF-sputtering with a Ni target and RF-PECVD following a procedure similar to that described elsewhere [15–20]. The used experimental arrangement consisted of a steel sample chamber connected to two rotary and diffusion pumps, and two electrodes of different area size; the smallest electrode was a nickel target electrode with a diameter of 7.5 cm and powered by a RF power supply. The other electrode, with 13 cm in diameter, was grounded through the body of the stainless steel chamber (see a schematic representation of this experimental arrangement in Fig. 1). In these experiments, the power supply with a power of 250 W and a frequency of 13.56 MHz was applied in a capacitive manner to the electrodes that were positioned at a separation distance of 5 cm. After reaching a background vacuum of about 10^{-5} mbar prior to the deposition, the pressure was raised at pressure of 0.025 mbar using only acetylene gas. Then, with this pressure, the deposition was started at room temperature over the grounded electrode on $1\text{ cm} \times 1\text{ cm}$ glass and silicon substrates. The pressure into the sample chamber was monitored during the deposition process to study the different stages of the deposition. The deposition time was varied (7, 10 and 13 min) to observe any change in the properties of the resulting films. The final samples were named A, B and C, respectively.

The surface morphology properties of the three samples were studied by AFM on non-contact mode, determining the average nanoparticles size and the root mean square (RMS) roughness. X-ray diffraction analysis was carried out using a X-ray powder diffractometer with Cu K_{α}

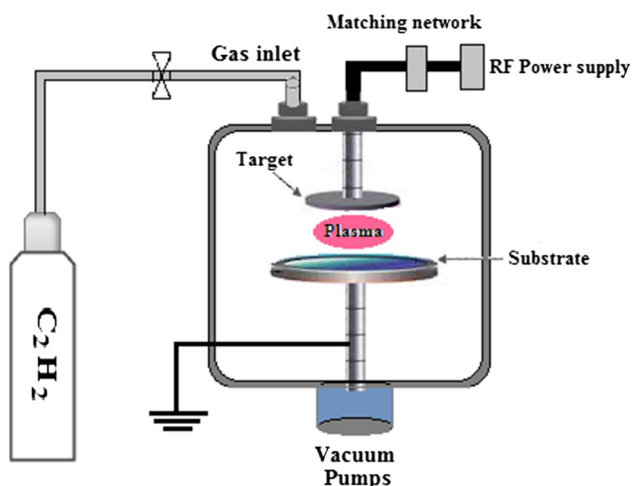


Fig. 1 Schematic representation of the experimental arrangement used in the preparation of the samples

radiation ($\lambda = 1.54060\text{ \AA}$) to identify the crystalline phases present in the samples. Also, the crystal sizes of the sample C was estimated calculating the mean coherence lengths, L , associated to the more intense diffraction peaks from the full width at half maximum (FWHM) of the aforesaid peaks with the Scherrer equation [21]:

$$L = \frac{0.9\lambda}{\beta \cos\theta_B} \quad (1)$$

where λ is the X-ray wavelength, β is the broadening of the diffraction peak (after subtracting the instrumental broadening) and θ_B is the Bragg angle at which the peak appears. The hysteresis loops at room temperature applying dc magnetic fields with a maximum applied field of 0.2 T were performed using a magnetometer. Finally, the electrical resistivity and its dependence on the presence of a magnetic field were measured using the van der Paw method and the usual 4-probe technique at room temperature [18].

3 Results and discussion

The deposition process of nickel nanoparticles in a regime with constant power of 250 W was investigated monitoring the sputtering conditions, particularly, the dependence of the pressure in the sample chamber, P , on the deposition time, t_d . Figure 2 shows this dependence for samples A and B. It is observed that the monitored pressure displays a non-monotonous variation with t_d ; firstly, during about the first half minute of the process (until the point 1 in the figure), P rapidly increases with increasing t_d . Then, P bears a descending stage until the fifth minute of deposition (point 2 in the figure), and thereafter P increases again with a low rate. We tentatively explain this tendency as follows.

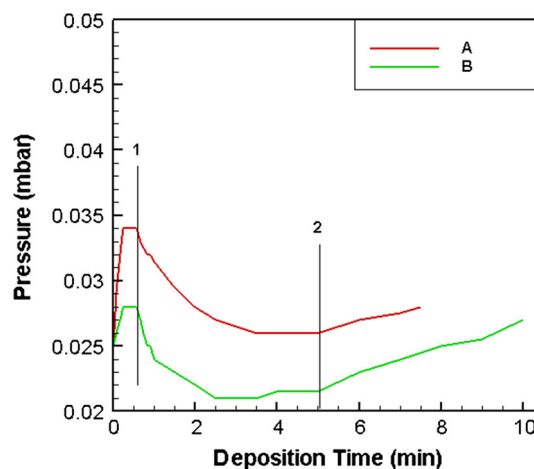


Fig. 2 Pressure inside the chamber during the process of deposition for samples A and B

At 0.025 mbar (the starting pressure), the mean kinetic energy of hydrocarbon ions is sufficient for physical sputtering the Ni target. Therefore, the pressure of the sample chamber increases due to the presence of sputtered Ni atoms. The increasing of P continues until the mean ion energy is reduced below the threshold energy of physical sputtering. This point is the cutoff the nickel target sputtering, consequently, P decreases, however the deposition of carbon continues and a small reactive sputtering of Ni target may also occur.

Figures 3a–c depicts AFM images of the three samples showing the nanostructures character of the films. The topographical curves, which indicate the distribution of the nanoparticles size, were obtained from these AFM studies (Fig. 3d). The cusp of these curves can be associated to the average diameter of the particles while its wideness refers to the variance; consequently, a sharper peak implies a low polydispersity degree. Samples A and B exhibited very similar particle size distributions with a narrow peak and an

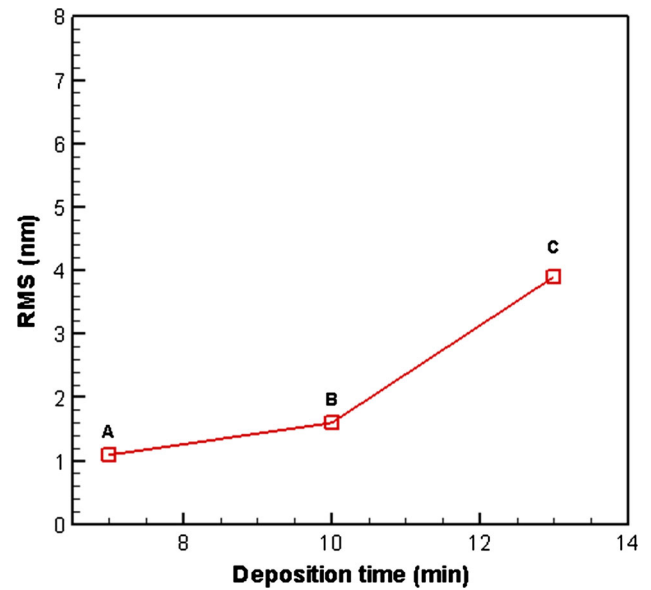
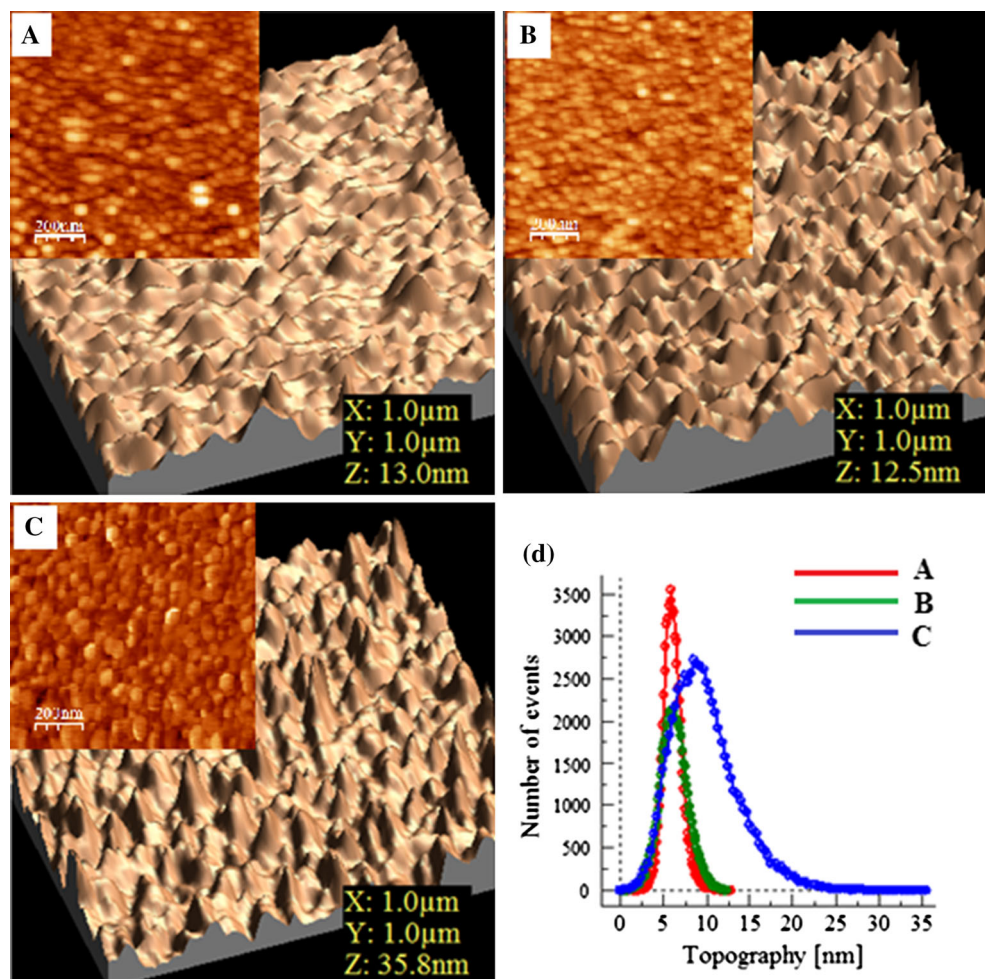


Fig. 4 Surface roughness of the samples versus deposition time

Fig. 3 a–d AFM images of the nickel samples (A, B and C), and d the corresponding size distribution of the particles



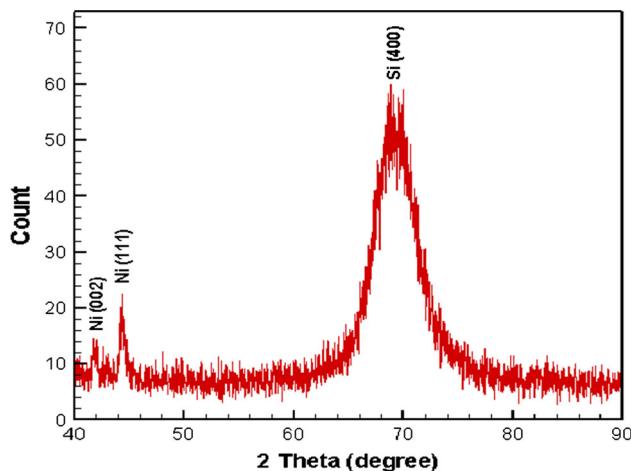


Fig. 5 XRD of the sample C

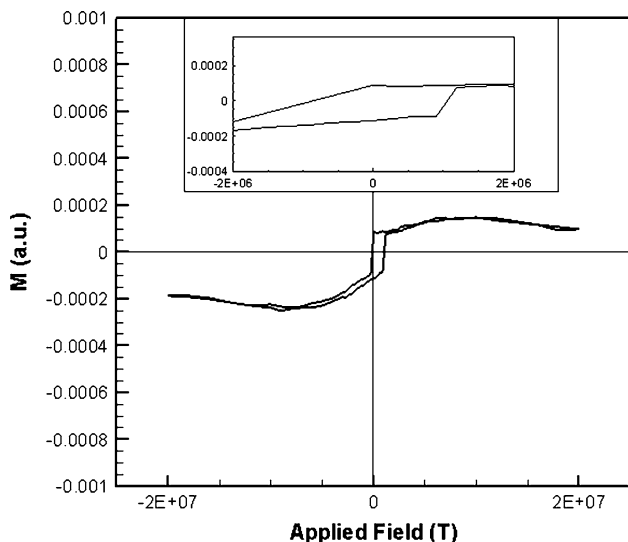


Fig. 6 Magnetic field dependence of the magnetization of sample C obtained at room temperature

average diameter around 6 nm, whereas for sample C the size distribution was broader and the average radius was of around 10 nm. In addition, the RMS of surface roughness over an area of 1000 nm × 1000 nm was also obtained from the AFM data as a function of the deposition time (Fig. 4). This dependence confirmed that the samples with more and bigger nanoparticles exhibit more surface roughness.

XRD pattern of the sample C, displayed intense diffraction peaks at $2\theta \approx 41^\circ, 44.5^\circ$ and 70° , which are ascribed to the crystalline phases present in the samples (Fig. 5). Concretely, besides the peaks corresponding to silicon substrate, peaks associated to the (111) and (002) planes of the face-centered cubic (fcc) phase of the metallic nickel (JCPDS 004-0850 and JCPDS 045-1027) were observed. Interestingly, no evidence of the presence of nickel oxide was observed, suggesting that part of the deposited carbon coated the Ni nanoparticles and avoid further sample oxidation in air. The estimated mean coherence lengths (L) associated to the (111) Ni peak using the Scherrer equation gave out 18 nm.

For sample C, the isothermal dependence of the magnetization on the applied magnetic field showed magnetic hysteresis loops at room temperature (Fig. 6), with coercive fields of around 0.01 T indicating that the particles have sizes above the critical particle size for the appearance of superparamagnetism [22].

Figure 7 depicts the magnetoresistance (MR) of Ni nanoparticles arrays as a function of the deposition time and the presence of a magnetic field. The MR could be calculated by Eq. 2.

$$MR = \frac{R(H) - R(H = 0)}{R(H = 0)} = \frac{\Delta R}{R} \tag{2}$$

It is observed that the MR decreases as the deposition time increases and more percentage of nickel in the films. This decaying resistivity for the films comprised of both

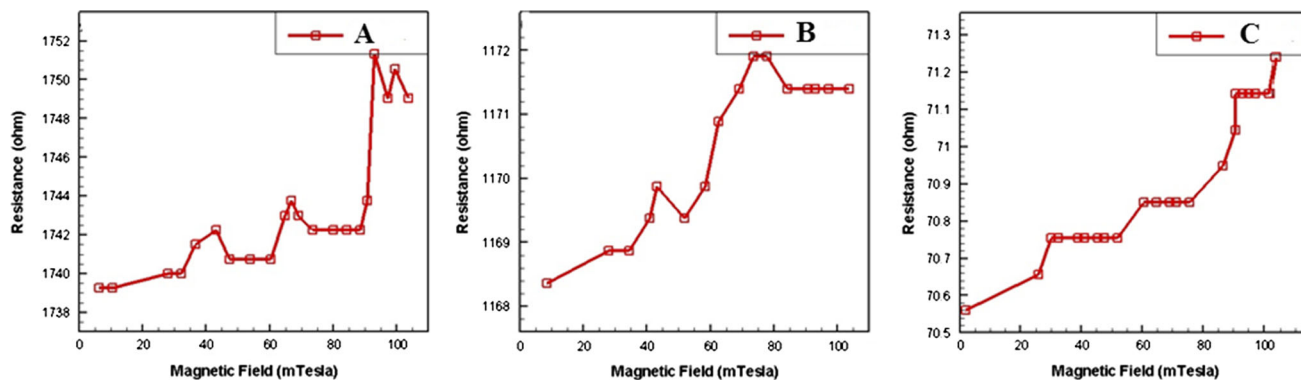


Fig. 7 Electrical resistivity of the samples obtained at different deposition time as functions of the applied magnetic field

metallic and insulating phases is tentatively explained considering simultaneously hopping effects and tunneling between isolated conducting clusters. In this manner, for the sample with less Ni deposition (sample A), it is expected that the electron tunneling between isolated Ni nanoparticles governs the conductivity of the film. However, as the deposition time is increased, the nickel content of the composite films gradually increases, leading to the formation of continuous paths of Ni particles exceeding the percolation threshold. Bi-dimensional (2D) AFM images of nanoparticle Ni/C composite films in different regimes of conductivity are shown in the insets in Fig. 3. Paying careful attention to the details of these images, it is appreciated how the concentration of Ni nanoparticles and their size increase as the deposition time is increased.

On the other hand, the values of the MR for the three samples significantly increased in the presence of magnetic fields, as the magnetic moments of the nanoparticles were aligned by the exciting magnetic field. In this process, not only the magnetic moment of the nanoparticles could rotate (Néel rotation) but also mechanical movements of the nanoparticles into the soft amorphous carbon film could occur. On the other hand, the magnitude of MR, determined as the ratio $\Delta R/R$, were 0.65, 0.26 and 0.20 % for samples A, B and C, respectively, indicating that $\Delta R/R$ decreases as the Ni nanoparticle concentration and Ni nanoparticle size were increased, probably due to the contribution of collective effects arising from inter particle interactions.

4 Conclusions

In the present contribution, it has been shown that the combination of the methods of accumulative chemical vapor deposition and radio waves sputtering represents a suitable route to prepare thin nanocomposite films constituted by Ni NPs arrays embedded into the amorphous carbon matrix showing interesting and tunable physical properties. Particularly, the control of the Ni NPs content and the Ni NPs size by adjusting the deposition time, versatily allows the modification of the electrical resistivity more than one order of magnitude (from around 70 to 1740 Ω). This experimental fact has been tentatively explained considering a combination of hopping and tunneling effects. On the other hand, the values of the

electrical resistivity of the nanocomposite films significantly increase as the magnetic moments of the nanoparticles are aligned by the presence of an exciting magnetic field ($\Delta R/R \approx 0.65\text{--}0.20\%$).

References

1. Frontiers of Nanoscience. in *Nanostructured Materials*, vol. 1, ed. by G. Wild. Elsevier (2009)
2. S. Sun, C.B. Murray, D. Weller, L. Folks, A. Moser, *Science* **287**(5460), 1989–1992 (2000)
3. J. Gao, H. Gu, B. Xu, *Acc. Chem. Res.* **42**(8), 1097–1107 (2009)
4. J.B. Haun, T.J. Yoon, H. Lee, R. Weissleder, *Wiley Interdiscip. Rev. Nanomed. Nanobiotechnol.* **2**(3), 291–304 (2010)
5. C.L. Criado, *J. Nanomed. Res.* **1**(1), 0005 (2014). doi:[10.15406/jnmr.2014.01.00005](https://doi.org/10.15406/jnmr.2014.01.00005)
6. S. Karmakar, S. Kumar, R. Rinaldi, G. Maruccio, *J. Phys. Conf. Ser.* **292**(1), 012002 (2011)
7. M. Vazquez, C. Luna, M.P. Morales, R. Sanz, C.J. Serna, C. Mijangos, *Phys. B* **354**(1), 71–79 (2004)
8. R. Mendoza-Reséndez, C. Luna, E.D. Barriga-Castro, P. Bonville, C.J. Serna, *Nanotechnology* **23**(22), 225601 (2012)
9. V.M. Prida, J. García, L. Iglesias, V. Vega, D. Görlitz, K. Nielsch, C. Luna, *Nanoscale Res. Lett.* **8**(1), 1–7 (2013)
10. A. Gelali, A. Ahmadpourian, R. Bavadi, M.R. Hantehzadeh, A. Ahmadpourian, *J. Fusion Energy* **31**, 586–590 (2012)
11. S. Țălu, S. Stach, S. Solaymani et al., *J. Electroanal. Chem.* **749**, 31–41 (2015)
12. V. Skumryev, S. Stoyanov, Y. Zhang, G. Hadjipanayis, D. Givord, J. Nogues, *Nature* **423**(6942), 850–853 (2003)
13. Y. Sun, M.B. Salamon, K. Garnier, R.S. Averback, *Phys. Rev. Lett.* **91**(16), 167206 (2003)
14. J. Kong, A.M. Cassell, H. Dai, *Chem. Phys. Lett.* **292**(4), 567–574 (1998)
15. S. Solaymani, S.M. Elahi, N.B. Nezafat, H. Zahrabi, A. Boochani, M. Naseri, *Eur. Phys. J. Appl. Phys.* **64**, 11301 (2013)
16. T. Ghodselahi, M.A. Vesaghi, A. Shafiekhani, A. Baradaran, A. Karimi, Z. Mobini, *Surf. Coat. Technol.* **202**(12), 2731–2736 (2008)
17. T. Ghodselahi, M.A. Vesaghi, A. Gelali, H. Zahrabi, S. Solaymani, *Appl. Surf. Sci.* **258**(2), 727–731 (2011)
18. T. Ghodselahi, A. Arman, *J. Mater. Sci. Mater. Electron.* **26**(6), 4193–4197 (2015)
19. M. Molamohammadi, A. Arman, A. Achour, B. Astinchap et al., *J. Mater. Sci. Mater. Electron.* (2015). doi:[10.1007/s10854-015-3170-5](https://doi.org/10.1007/s10854-015-3170-5)
20. S. Țălu, S. Stach, T. Ghodselahi, A. Ghaderi, S. Solaymani et al., *J. Phys. Chem. B* **119**(17), 5662–5670 (2015)
21. B.D. Cullity, S.R. Stock, *Elements of X-ray Diffraction*, 3rd edn. (Prentice Hall, 2001)
22. C. Luna, C.J. Serna, M. Vázquez, *Nanotechnology* **14**(2), 268 (2003)